*Natural Resources Research, Vol. 29, No. 1, February 2020 (© 2019)*
https://doi.org/10.1007/s11053-019-09526-0

*Original Paper*

# Estimating Model Parameters from Self-Potential Anomaly of 2D Inclined Sheet Using Whale Optimization Algorithm: Applications to Mineral Exploration and Tracing Shear Zones

**Mohamed Gobashy,[1,3] Maha Abdelazeem,[2] Mohamed Abdrabou,[1] and Mohamed H. Khalil[1]**

*Received 11 May 2019; accepted 18 July 2019*
*Published online: 27 July 2019*

The use of spontaneous potential (SP) anomalies is well known in the geophysical literatures because of its effectiveness and significance in solving many complex problems in mineral exploration. The inverse problem of self-potential data interpretation is generally ill-posed and nonlinear. Methods based on derivative analysis usually fail to reach the optimal solution (global minimum) and trapped in a local minimum. A new simple heuristic solution to SP anomalies due to 2D inclined sheet of infinite horizontal length is investigated in this study to solve these problems. This method is based on utilizing whale optimization algorithm (WOA) as an effective heuristic solution to the inverse problem of self-potential field due to a 2D inclined sheet. In this context, the WOA was applied first to synthetic example, where the effect of the random noise was examined and the method revealed good results using proper MATLAB code. The technique was then applied on several real field profiles from different localities aiming to determine the parameters of mineralized zones or the associated shear zones. The inversion parameters revealed that WOA detected accurately the unknown parameters and showed a good validation when compared with the published inversion methods.

**KEY WORDS:** Spontaneous potential inversion, Whale algorithm, Artificial intelligence, 2D inclined sheet, Mineralization, Shear zones.

## INTRODUCTION

Because of its success and accuracy in numerous applications, the use of spontaneous potential (SP) anomalies is prevalent in some geophysical applications especially those related to mineral exploration and similar natural resources. It is a passive method that mainly based on the measurement of the natural potentials resulted from electrokinetic or electrochemical reactions. The obtained measurements are natural potentials caused by subsurface electrical properties. These potentials demonstrated in millivolts (mV) that acquired via two electrodes planted on the earth's surface. Consequently, the acquisition of SP technique is capable of locating bodies by the interpretation of their anomalies qualitatively and quantitatively. SP method has appreciable significance in geothermal exploration (Zlotnicki and Nishida 2003), sulfide and graphite exploration (Mendonca 2008; Biswas 2019),

[1]Geophysics Department, Faculty of Science, Cairo University, Giza, Egypt.
[2]National Research Institute of Astronomy and Geophysics (NRIAG), Helwan, Cairo, Egypt.
[3]To whom correspondence should be addressed; e-mail: Bouguer3000@yahoo.com

groundwater investigations (Titov et al. 2015), dam and embankment seepage control (Black and Corwin 1984; Moore et al. 2011), archeological investigations (Drahor et al. 1996; Drahor 2004) and detection of landfill leachate (Arora et al. 2007). The SP anomaly observed in the field could be contributed to single buried source geometries (sphere, horizontal cylinder and vertical cylinder) (El-Araby 2004; El-Kaliouby and Al-Garni 2009) and/or 2D inclined sheet model which represents one of the often utilized models for the interpretation of self-potential anomalies resulted from ore deposits (Paul 1965; Murty and Haricharan 1985).

In general, the process of quantitative interpretation of SP anomalies has been discussed by several methods that can be classified into two classes. The first class comprises methods based on continuous modeling of SP data of 2D and 3D geological bodies (Guptasarma 1983; Shi and Morgan 1996; Mendonca 2008), which requires density and electric current resistivity in their application. Solving of 2D and 3D self-potential inverse modeling requires some knowledge (a priori information) about source parameters like the acquired depth via independent geophysical and/or geological information (Abdelrahman et al. 2003) and complete solution of the forward model. The second class uses fixed modeling of simple geometric bodies, such as 2D inclined sheet, vertical cylinder, sphere and horizontal cylinder, where the shape of the subsurface body and depth are determined from measured SP data at the surface of the earth. This class does not reflect the actual subsurface buried body; nevertheless, it gives reasonable outcomes to perform the process of interpretation with the inverted SP data close to the measured one. The benefits of the second class are that it requires only SP data and does not need the knowledge of the depth approximation, resistivity distribution and/or the current density.

Numerous techniques have been developed to evaluate the model unknown parameters (polarization amplitude, the zero distance from origin, the polarization angle, depth and the shape factor or half-width) of the subsurface source body from surface SP measurements along a profile. Those contain approaches such as logarithmic curve matching (Murty and Haricharan 1984), the use of derivative analysis method (Abdelrahman et al. 1998) utilizing the characteristic points, distances, curves and nomogram method (Atchuta Rao and Ram Babu 1983; Murty and Haricharan 1985; Babu and Rao 1988) and the utilization of spectral analysis (Rani et al. 2015). Moreover, genetic algorithms (Abdelazeem and Gobashy 2006), particle swarm optimization (Monteiro Santos 2010), differential evolution (Li and Yin 2012), very fast simulated annealing (Biswas and Sharma 2014a, b, 2015, 2016) and black hole algorithm (Warnana 2018) were used to interpret self-potential observed data.

In the present work, a global meta-heuristic optimization algorithm was used to perform interpretation of SP anomalies resulted from two-dimensional inclined sheet like model. This technique is based on using whale optimization algorithm (WOA) (Mirjalili and Lewis 2016) that solves for five parameters of the buried sheet, namely the polarization amplitude ($K$), the zero distance from origin ($x_a$), the depth to the sheet center ($h$), the polarization angle ($\alpha$) and the half-width of the sheet ($a$). This algorithm is simple in its concept and has several advantages. These includes: (1) this algorithm does not require adjusting of tuning parameters like particle swarm optimization (PSO) and genetic algorithm (GA) which represent a limiting factor when applying those algorithms, (2) there is no need for training, which is an important step that takes more time in modular neural network (MNN) technique (El-Kaliouby and Al-Garni 2009) and (3) this algorithm is very fast during calculation and inversion. This paper started with the forward model and then a description of the proposed algorithm. Afterward, the tested noise-free theoretical example and noisy example were discussed. Finally, the application of this artificial intelligence algorithm on some real field examples was presented.

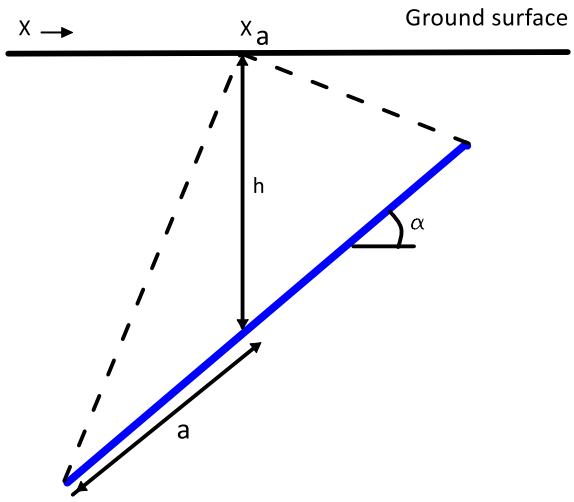


**Figure 1.** Explanation of 2-D inclined sheet model parameters.

## Problem Formulation and Forward Model

The formula expressing the self-potential anomaly at any surface point $V(x)$ along a line normal to the strike of a 2D inclined sheet model (Fig. 1) (Murty and Haricharan 1985; Sundararajan et al. 1998) is given as:

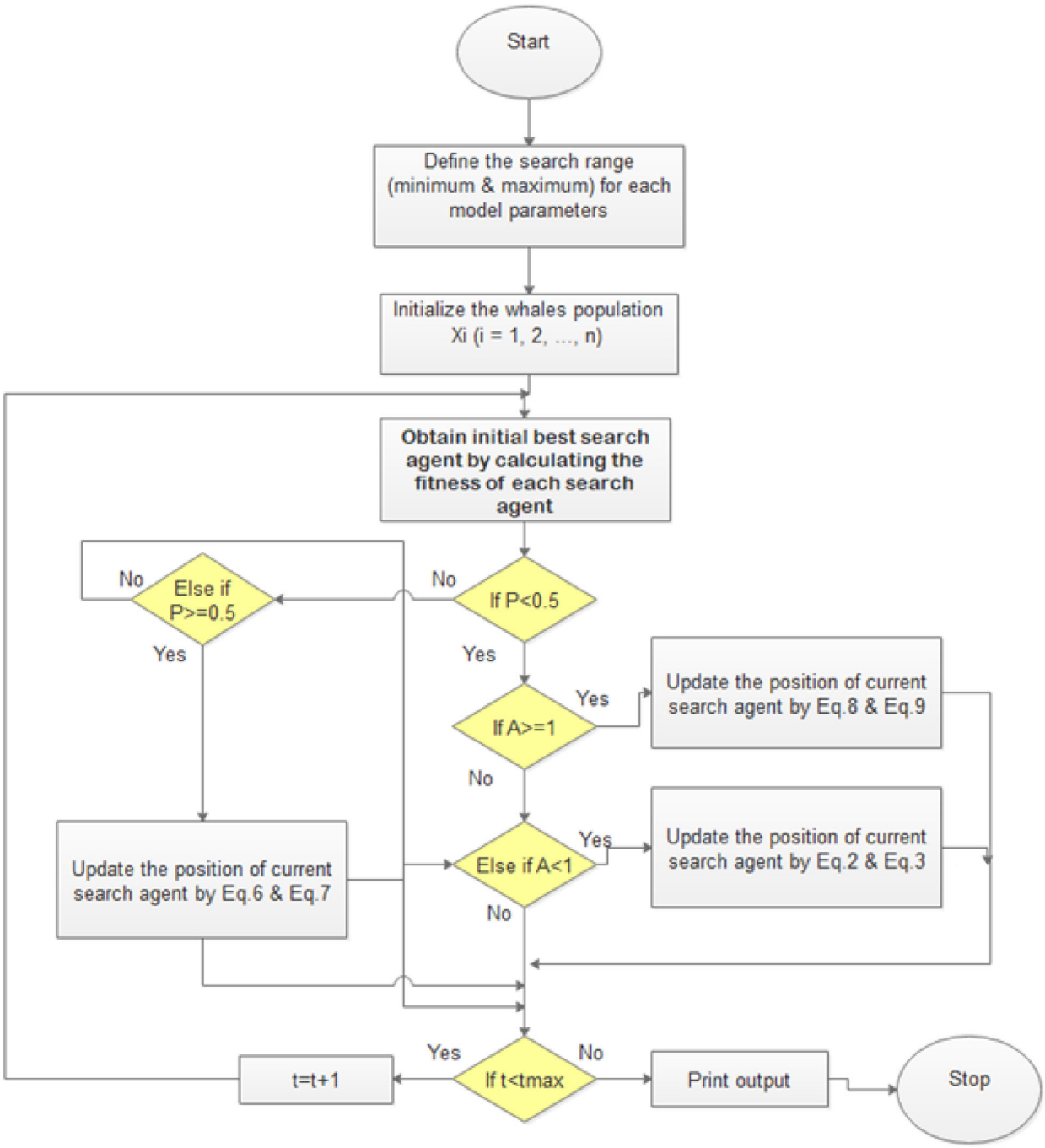


**Figure 2.** Flow chart of the WOA algorithm for the inversion of SP data. Here, $t$ refers to iteration and $t_{max}$ is the maximum iteration.

$$V(x) = k \ln \left[ \frac{\{(x - x_a) - a \cos \alpha\}^2 + (h - a \sin \alpha)^2}{\{(x - x_a) + a \cos \alpha\}^2 + (h + a \sin \alpha)^2} \right] \quad (1)$$

In the above equation, $k$ is the polarization amplitude, $x_a$ is the horizontal location of the sheet center, $h$ refers to the depth to the sheet center, $a$ denotes the half-width of the sheet and $\alpha$ defines the inclination angle. The above formulation solves for the forward problem required through the process of inversion and objective function design ($V_i^c$: computed SP data of the model in Eq. 10).

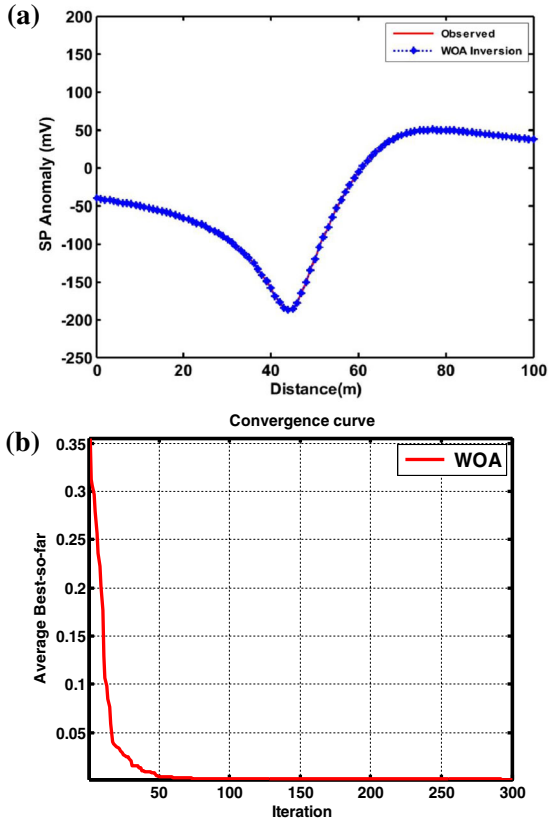


**Figure 3.** WOA inversion results for synthetic SP anomaly of 2-D inclined sheet model. **(a)** Comparison between inverted response (blue) and synthetic data (red), **(b)** convergence curve of the objective function with WOA iterations values.

## Whale Optimization Algorithm (WOA)

The whale optimization algorithm (WOA) is a meta-heuristic algorithm that was first designated by (Mirjalili and Lewis 2016). WOA was tested with 29 mathematical optimization problems and classical engineering problems and showed good results (Mirjalili and Lewis 2016). The benefits of this algorithm are simplicity and low computational cost. Optimization outcomes showed that the WOA is very competitive when compared with the meta-heuristic algorithms, such as gravitational search algorithm (GSA) and particle swarm optimization (PSO) as well as conventional methods.

WOA was inspired from nature that simulates the humpback whale behavior. They can identify the position of prey (school of small fishes) and surround them. Where the optimal position in the search range is unknown a priori, the WOA presumes that best solution is the objective prey (i.e., target) or is near to the best. After initializing the optimum search agent, the further search agents (solutions) will attempt to enhance their positions following the optimum solutions. Such position update is represented by (Mirjalili and Lewis 2016):

$$\vec{D} = |\vec{C} \cdot \overrightarrow{X^*}(t) - \vec{X}(t)| \quad (2)$$

$$\vec{X}(t+1) = \overrightarrow{X^*}(t) - \vec{A} \cdot \vec{D} \quad (3)$$

**Table 1.** True and inverted model parameters using WOA due to a 2D inclined sheet model

| Parameter | $K$ (mV) | $X_a$ (m) | $a$ (m) | $\alpha$ (°) | $h$ (m) | Misfit error (%) |
|---|---|---|---|---|---|---|
| True model | 50 | 55 | 12 | 150 | 10 | – |
| Noise-free | 50.34 | 54.94 | 11.91 | 149.92 | 10.03 | 0.0767 |
| 10% noise | 49.995 | 54.889 | 11.985 | 149.85 | 10.08 | 0.3079 |
| 20% noise | 42.97 | 56 | 13.88 | 151.91 | 9.63 | 1.8321 |
| 30% noise | 59.91 | 53.78 | 10.23 | 149.06 | 10.95 | 2.1096 |

The search spaces for WOA are: – 200:200 mV ($K$), 0:100 m ($X_a$), 1:40 m ($a$), 0:180° ($\alpha$) and 0:40 m ($h$)

where $t$ refers the iteration, $\vec{A}$ and $\vec{C}$ are coefficient vectors, $\overrightarrow{X^*}$ refers to the current optimal solution position vector, $\vec{X}$ defines the new position vector, $\vec{D}$ refers to the distance vector separates between the whale and prey, | | defines the absolute value and '·' refers to the element-wise multiplication. It is important to note that $\overrightarrow{X^*}$ is updated in each iteration if a better solution is found. Each whale is regarded as a solution for the cost function (Eq. 10) in the process of optimization. Depending on the value of the objective function, the optimal solution is determined. The coefficient vectors $\vec{A}$ and $\vec{C}$ are calculated through Eqs. 4 and 5:

$$\vec{A} = 2\vec{a} \cdot \vec{r} - \vec{a} \tag{4}$$

$$\vec{C} = 2 \cdot \vec{r} \tag{5}$$

where $\vec{a}$ is reduced linearly from 2 to 0 along the generations and $\vec{r}$ is a random vector in [0, 1].

The meta-heuristic optimization algorithms split a common property irrespective of their nature. The search process is fractionated into two phases: the exploitation phase and the exploration phase.

### Exploitation Phase

In the WOA, exploitation phase was represented by attacking bubble-net humpback whales' behavior, in which two mechanisms were delineated (shrinking mechanism and updating of spiral position). The mechanism of shrinking surrounding was accomplished by reducing the value of $\vec{a}$ in Eq. 4. Winding upgrading position was achieved by first calculating the separation linking the whale sited at $\vec{X}$ and target prey sited at $\overrightarrow{X^*}$. After that, the winding equation was formulated between the position of whale and prey (optimum solution) to simulate the helical movement of humpback whales via this formula (Mirjalili and Lewis 2016):

$$\vec{X}(t+1) = \overrightarrow{D'} \cdot e^{bl} \cdot \cos(2\pi l) + \overrightarrow{X^*}(t) \tag{6}$$

where $\overrightarrow{D'} = |\overrightarrow{X^*}(t) - \vec{X}(t)|$ and refers to the separation vector between the $i$th whale to the target (the optimal solution), $b$ denotes a constant that describes the shape of the logarithmic spiral, $l$ defines a random number in $[-1, 1]$ and '·' refers to the element-wise multiplication. Since the whales surround about the prey (best solution) through a shrinking circle and through a helical-shaped path concurrently, we suppose a probability equals 50% was present for the choice either between the shrinking mechanisms or between the spiral upgrading mechanisms to improve the solution in

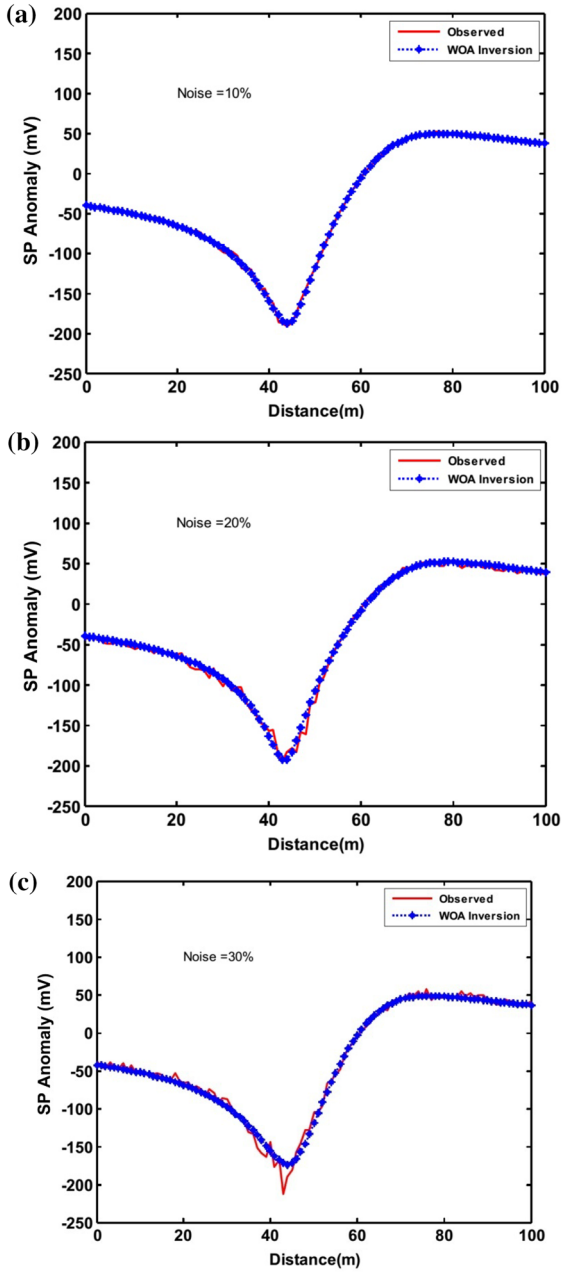


**Figure 4.** Synthetic SP anomaly of 2-D inclined sheet model with their WOA inversion responses for (**a**) with 10% of random noise, (**b**) with 20% of random noise and **c** with 30% of random noise.

**Table 2.** Comparison between the WOA and SA, GA and BHA algorithms

| | $K$ (mV) | $X_a$ (m) | $h$ (m) | $a$ (m) | $\alpha$ (°) | Misfit error (%) | Fval | Iterations | Time (s) |
|---|---|---|---|---|---|---|---|---|---|
| True model | 50 | 55 | 10 | 12 | 150 | – | – | – | – |
| SA | 142.91 | 52.41 | 12.86 | 4.79 | 145.44 | 3.05 | 0.11 | 8576 | 308 |
| GA | 42.84 | 56.46 | 6.56 | 15.72 | 141.75 | 3.86 | 0.03 | 626 | 1005 |
| BHA | 56.06 | 53.94 | 10.56 | 10.94 | 147.91 | 1.15 | 0.08 | 300 | – |
| Sungkono (2018) (5% noise). | | | | | | | | | |
| WOA | 49.99 | 54.88 | 10.08 | 11.98 | 149.85 | 0.3 | 0.03 | 300 | 14.464 |

As applied on a 2D inclined sheet model ($K$ = 50 mV, $X_a$ = 55 m, $h$ = 10 m, $a$ = 12 m and $\alpha$ = 150°) and profile length = 101 units with 1-unit interval) with 10% noise

*SA* simulated annealing, GA genetic algorithm, *BHA* black hole algorithm

Fval: minimum objective function value at optimum solution

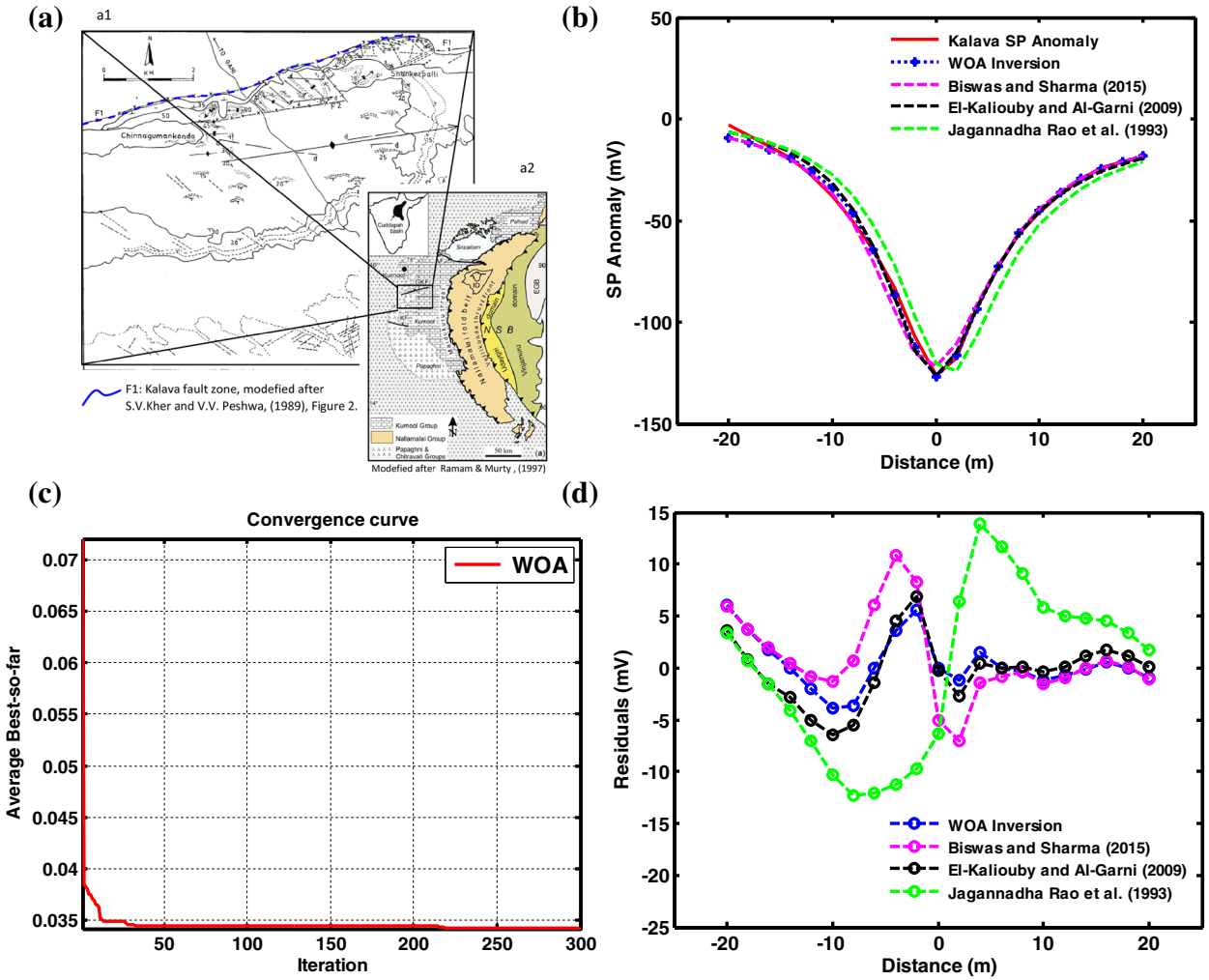


**Figure 5.** WOA results for Kalava SP anomaly (Rao et al. 1982). (**a**) Sketch of the geological map of the Cuddapah Basin showing the sub-basins [after Ramam and Murty 1997, where GKF, Gani–Kalava fault; AF, Atmakur fault; KF, Kona fault; NSB, Nallamalai (a2) and Kher and Peshwa 1989 (a1)], (**b**) estimated data from WOA, other methods (Jagannadha Rao et al. 1993; El-Kaliouby and Al-Garni 2009; Biswas and Sharma 2015) and measured data (red), (**c**) cost function with iterations, and (**d**) residuals between measured SP response and inverted anomaly from WOA and other methods.

the process of optimization. This could be described through the following form (Mirjalili and Lewis 2016):

$$\vec{X}(t+1) = \begin{cases} \overrightarrow{X^*}(t) - \vec{A}.\vec{D} & \text{for } p < 0.5 \\ \overrightarrow{D'} \cdot e^{bl} \cdot \cos(2\pi l) + \overrightarrow{X^*}(t) & \text{for } p \geq 0.5 \end{cases} \quad (7)$$

here, $p$ refers to a random number in the space [0, 1] and $\vec{X}$ is the updated solution.

### Exploration Phase

This phase included the process of searching for target prey. Since the search, process that whales do is random in reality, the utilization of $\vec{A}$ with the random values $> 1$ will force the search agent to go aside from a reference whale. In contrast to the exploitation phase, the position of the search agent was upgraded through the randomly chosen search agent rather than the optimum search agent reached. Using $|\vec{A}| > 1$ highlights the exploration phase and prevents the WOA to fall in the local minimum and to reach the global minimum search. This process could be expressed as (Mirjalili and Lewis 2016):

$$\vec{D} = |\vec{C} \cdot \overrightarrow{X_{\text{rand}}} - \vec{X}| \quad (8)$$

$$\vec{X}(t+1) = \overrightarrow{X_{\text{rand}}} - \vec{A} \cdot \vec{D} \quad (9)$$

where $\vec{X}$ refers to the new position (i.e., new solution) and $\overrightarrow{X_{\text{rand}}}$ is defined as a random position vector. At last, the iteration will stop after the maximum iteration is done. The update of the position of the whales based on the global best solutions constructed at the final iteration. Eventually, the generation does not cease up to the obtained solution persuades the criteria of convergence (Fig. 2). Further discussion of the stability of this algorithm was investigated by Mirjalili and Lewis (2016).

The SP data in this work were inverted using the objective function given in Eq. 10 (Monteiro Santos 2010). The misfit between observed and computed SP data was estimated utilizing the average relative error percentage that was evaluated via Eq. 11:

$$Q = 2\left\|V_i^o - V_i^c\right\| / \left[\left\|V_i^o + V_i^c\right\| + \left\|V_i^o - V_i^c\right\|\right] \quad (10)$$

$$\text{Misfit Err}(\%) = (100/N)\sqrt{\sum_i^N [(V_i^o - V_i^c)/V_i^o]^2} \quad (11)$$

where $N$ refers to the number of observed SP readings, $V_i^o$ and $V_i^c$ denote the measured SP data and computed one, respectively. The above expression was found to be highly stable in optimizing the ill-posed SP problem.

We developed a software package Sp_WOA_inv to invert the objective function given in Eq. 10.

## RESULTS

### Synthetic Example

The WOA, proposed to infer the solution of the inverse problem of SP data, resulted from buried 2D inclined sheet structure. This algorithm has been used to invert a synthetic SP data assuming the model has the following parameters $k$ = 50 mV, $a$ = 12 m, $\alpha$ = 150°, $x_a$ = 55 m and, $h$ = 10 m, leading to the effect displayed in Figure 3a. The number of data points in this theoretical example was 101 points with 1-m interval between them. In the WOA inversion process, 200 search agents and 300 iterations were used to get the outcomes. The average

**Table 3.** WOA inversion results of Kalava Field anomaly (a comparison with other methods)

| Methods | $K$ (mV) | $X_a$ (m) | $a$ (m) | $\alpha$ (°) | $h$ (m) |
|---|---|---|---|---|---|
| Jagannadha Rao et al. (1993) | – | 0.4 | 3.75 | 80 | 7.59 |
| El-Kaliouby and Al-Garni (2009) | 68.29 | − 0.9 | 3.15 | 78.72 | 7.2 |
| Biswas and Sharma (2015) | − 867 | − 0.8 | – | 81.8 | 7 |
| WOA | 64.62 | − 0.455 | 3.35 | 82.42 | 7.35 |

The search spaces for WOA are: 50:100 mV ($K$), − 5:5 m ($X_a$), 1:7 m ($a$), 80:120° ($\alpha$) and 5:15 m ($h$)

best of the objective function is demonstrated in Figure 3b. The resulted parameters and inverted field were identical to the assumed ones. The maximum error of misfit was 0.0767% for the inversion of noise-free data, as tabulated in Table 1, along with parameter search ranges and the inverted outcomes.

The choice of the parameter search spaces was depended mostly on the observed data in the field. Master curves indicated that deeper bodies exhibited a wide curve, whereas shallower bodies exhibited a narrow curve. The uniformity of the curve anomaly was affected by the inclination angle of the

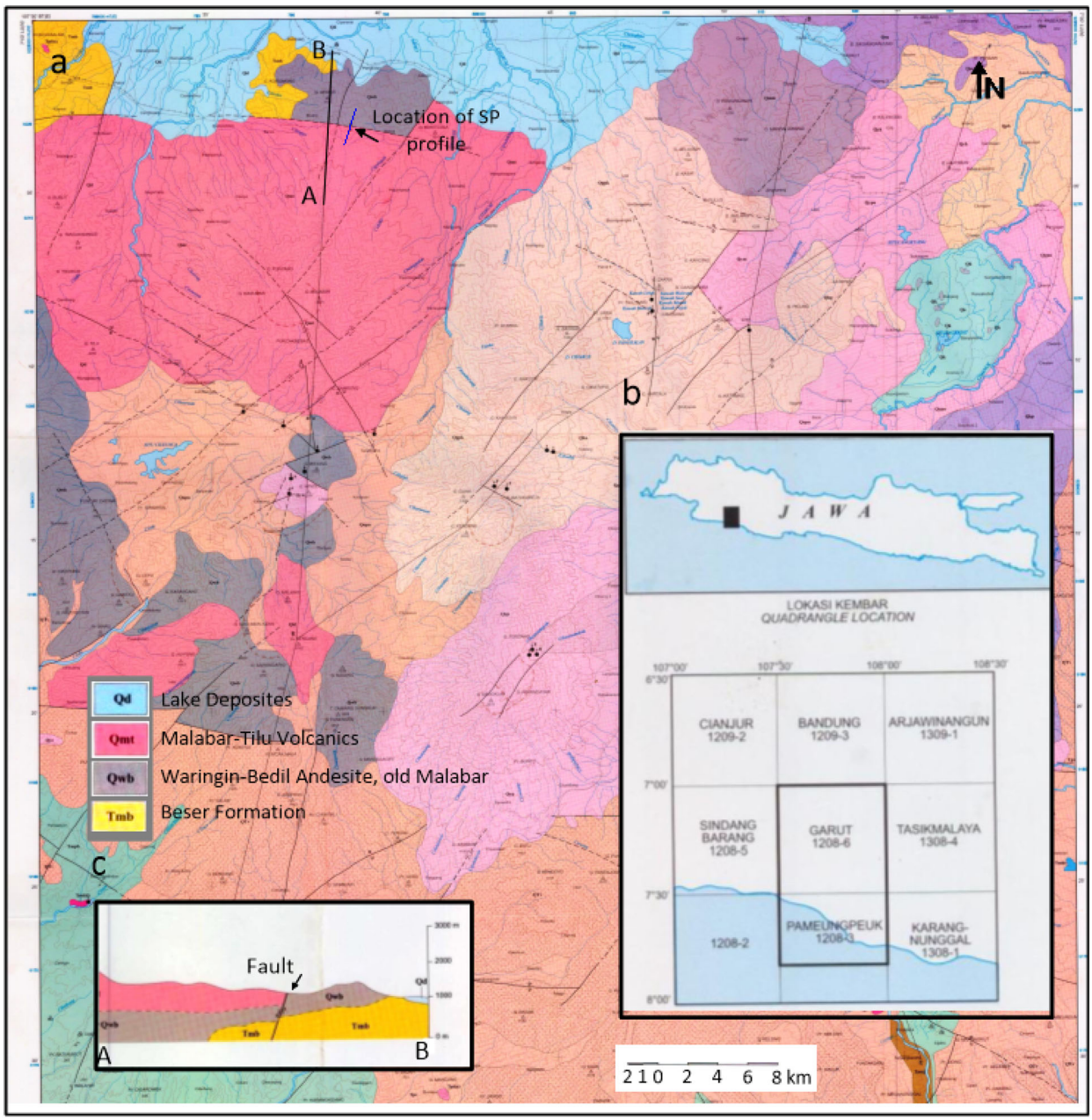


**Figure 6.** (**a**) General geology of Garut and Pameungpeuk quadrangle, (modified after Alzwar et al. 1992), showing the location of the SP anomaly profile and a cross-sectional view (**c**), and (**b**) general location of Garut Pameungpeuk quadrangle.

body. The inverted response is drawn together with synthetic SP data in Figure 3a.

*Analysis of Noisy Data*

In the interpretation of the real field data, the noise was a significant element to be considered. The aforementioned noise-free data have been tested with adding a maximum noise of 30%. The noisy data and the inverted ones of three different levels of noise 10, 20 and 30% are shown in Figure 4a, b and c, respectively. It could be noticed that the results obtained by WOA inversion of noisy data were sufficient and accurate until 30% random noise level as shown in Table 1.

*Comparison with Other Inversion Algorithms*

In this subsection, we compare the results obtained by the present WOA and some known algorithms working with different concepts. These include genetic algorithm (GA) as a global optimizer (Abdelazeem and Gobashy 2006; Göktürkler and Balkaya 2012), simulated annealing (SA) and black hole algorithm (BHA) to demonstrate the stability of WOA.

We computed SP anomaly [with random error percentage (10%)] due to a 2D sheetlike model ($K$ = 50 mV, $x_a$ = 55 m, $h$ = 10 m, $a$ = 12 m and $\alpha$ = 150°) and profile length = 101 units with 1-unit interval). We then apply the WOA, SA, GA and BHA to the same data. Numerical results are summarized in Table 2.

It is established numerically that the present proposed heuristic technique gives better results for all parameters than the other algorithms when using the same data [with 10% noise, except the BHA 5% after Sungkono (2018)]. A clear consistency can be observed between the WOA's calculated parameters and the true ones, leading to the lowest misfit error (0.03%) and the shortest elapsed time (14.464 s) to reach the solution. This demonstrates that WOA has significant improvements over the well-known global optimizers in its stability and consistency.

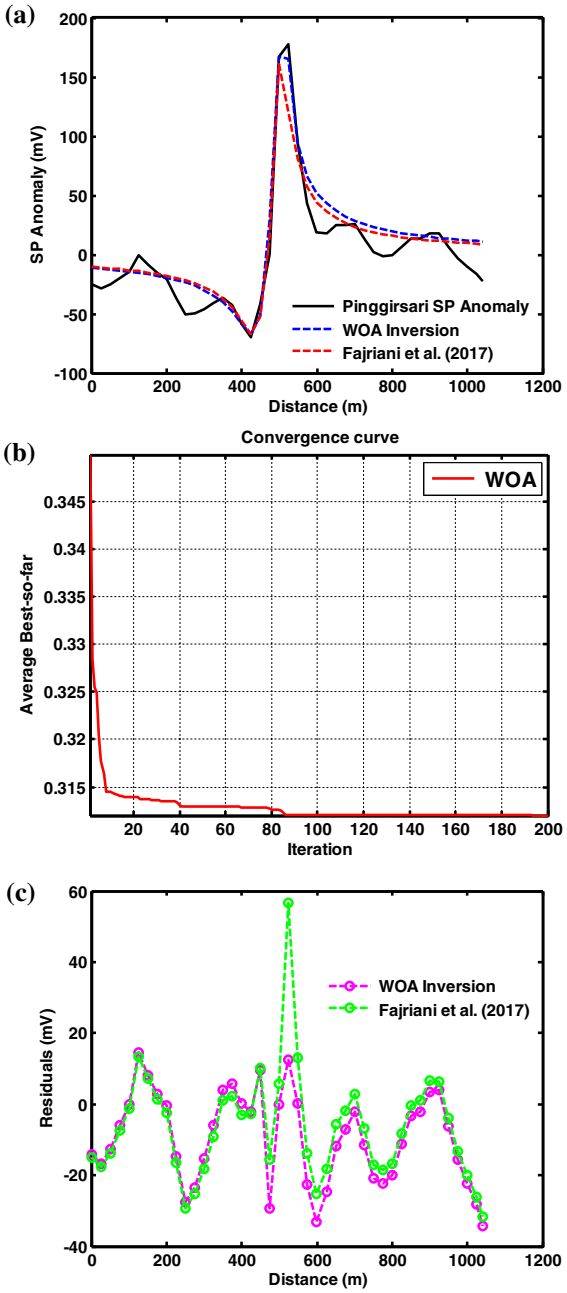


**Figure 7.** WOA results for Pinggirsari SP anomaly (Fajriani et al. 2017). (**a**) Calculated data from WOA (blue), from (Fajriani et al. 2017) (red) and measured SP data (black), (**b**) cost function with iterations, and (**c**) residuals between measured SP response and inverted SP response from WOA and (Fajriani et al. 2017).

**Table 4.** WOA inversion results of Pinggirsari SP anomaly

| Methods | $K$ (mV) | $X_a$ (m) | $a$ (m) | $\alpha$ (°) | $h$ (m) |
|---|---|---|---|---|---|
| Fajriani et al. (2017) | 41.5 | 478.25 | 34 | 334.52 | 14.63 |
| WOA | 47.38 | 479.625 | 35.85 | − 149.98 | 15.68 |

A comparison with other method is given. The search spaces for WOA are: 10:60 mV ($K$), 400:600 m ($X_a$), 20:60 m ($a$), − 200:0° ($\alpha$) and 0:20 m ($h$)

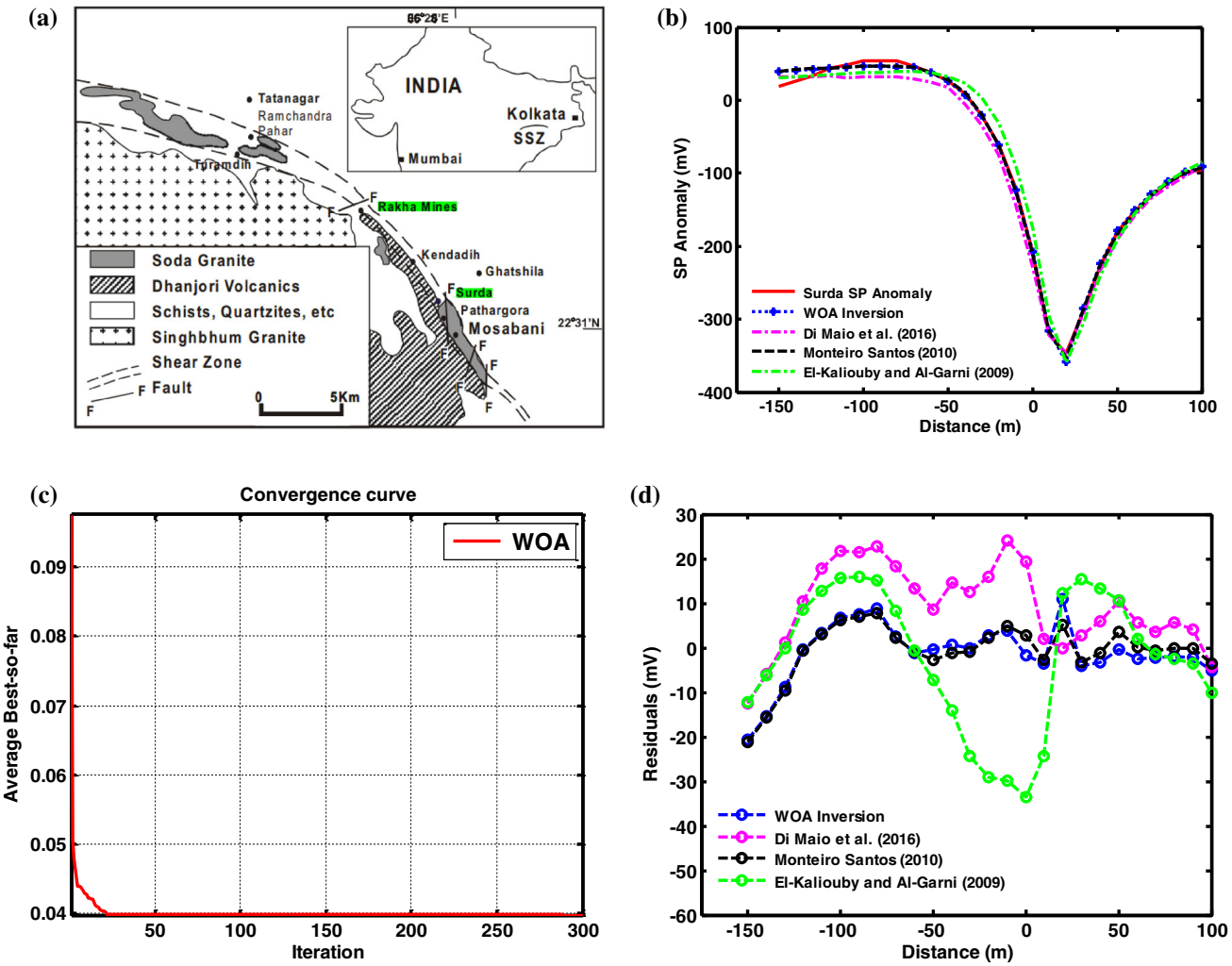


**Figure 8.** WOA inversion results for Surda SP anomaly (Murthy et al. 2005). (**a**) Regional geological map of the Singhbhum Shear Zone (SSZ) and location of the Mosabani and Rakha copper mines, East Singhbhum district. (Modified after Changkakoti et al. 1987), (**b**) obtained response from WOA, other methods (El-Kaliouby and Al-Garni 2009; Monteiro Santos 2010; Di Maio et al. 2016) and measured data (red), (**c**) objective function with iterations, (**d**) differences between measured SP data and calculated data from WOA and other methods.

**Table 5.** WOA inversion results of Surda SP anomaly

| Methods | $K$ (mV) | $X_a$ (m) | $a$ (m) | $\alpha$ (°) | $h$ (m) |
|---|---|---|---|---|---|
| El-Kaliouby and Al-Garni (2009) | 130.86 | 5.86 | 19.51 | 50.96 | 27.78 |
| Monteiro Santos (2010) | 98.38 | − 3.87 | 28.8 | 45.98 | 31.4 |
| Di Maio et al. (2016) | 128.67 | 1.72 | 21.92 | 52.47 | 31.94 |
| WOA | 94.57 | − 4.17 | 29.91 | 45.94 | 31.29 |

A comparison with other methods is given. The search spaces for WOA are: 90:180 mV ($K$), − 20:40 m ($X_a$), 10:30 m ($a$), 20:50° ($\alpha$) and 10:40 m ($h$)

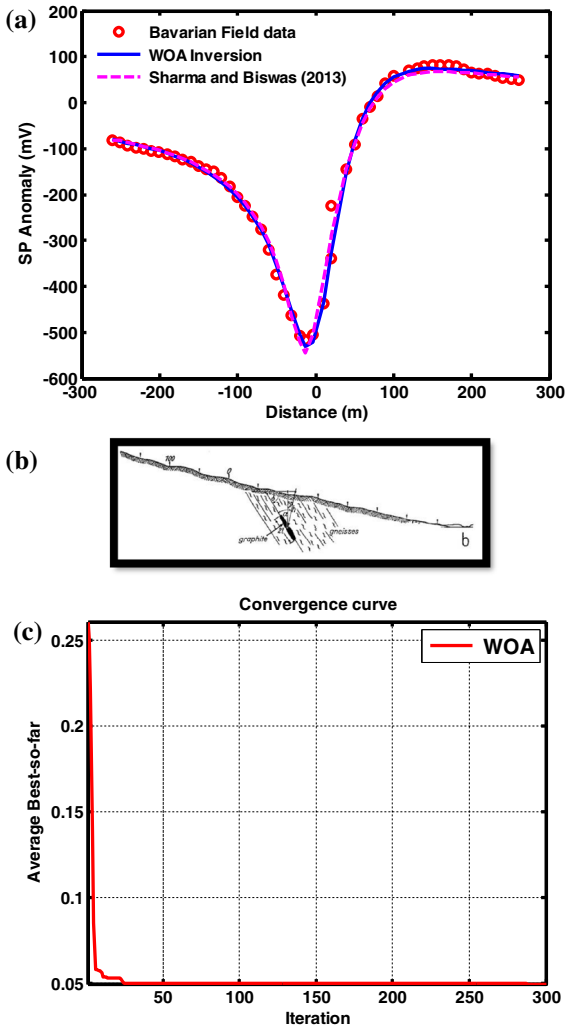


**Figure 9.** WOA inversion results for Bavarian Woods Field anomaly (after Meiser 1962). (**a**) Predicted response from WOA (Sharma and Biswas 2013) and measured data (red circles), (**b**) the corresponding geological cross section (after Meiser 1962), and (**c**) objective function with iterations.

## *Field Examples*

Field data from different localities were investigated to examine the capability and constancy of the WOA inversion.

## *Kalava Field Anomaly*

SP anomaly was taken across a mineralized belt in Kalava fault zone, 52 km south of Kurnool in Cuddapah Basin, Andhra Pradesh, India (Rao et al. 1982; Sanker Narayan et al. 1982). Cuddapah Basin (Fig. 5a) is characterized by quartzite–carbonate–shale cycles having an aggregate thickness that is estimated to vary between 6 and 12 km. The early sediments of the basin are interspersed with basic volcanics and sills. Felsic volcanics and tuffs are intercalated with sediments at many horizons. The basin is known for its mineral potential in the form of limestones and dolomites, bedded and vein barites, chrysotile asbestos and steatite, besides occurrences of base metals, diamond, phosphorite, uranium and abundant building and ornamental stones (https://www.ndrdgh.gov.in/NDR/?page_id=860, Sanker Narayan et al. 1982). Earlier drilling over some anomaly locations in this area by the Geological Survey of India encountered carbonaceous shales with sulphide mineralization. These might be the sources causing the SP anomaly under study. The geological environment of the Kalava Fault Zone is shown in the sketch geological map of the Cuddapah Basin (after Ramam and Murty 1997; Kher and Peshwa 1989) and displayed in Figure 5a (a1 and a2). The Kalava self-potential profile (Fig. 5b) was digitized at 2-m interval with profile length of 40 m. This field study was interpreted as

**Table 6.** WOA inversion results of Bavarian Woods SP anomaly

| Methods | $K$ (mV) | $X_a$ (m) | $a$ (m) | $\alpha$ (°) | $h$ (m) |
|---|---|---|---|---|---|
| Meiser (1962) | – | – | – | – | 53 |
| Sharma and Biswas (2013) | 158.3 | 20.5 | 44.6 | 134.3 | 50.9 |
| WOA | 221.068 | 17.026 | 32.523 | 132.777 | 49.516 |

A comparison with other methods is given. The search spaces for WOA are: 10:300 mV ($K$), – 50:50 m ($X_a$), 10:100 m ($a$), 0:180° ($\alpha$) and 10:100 m ($h$)

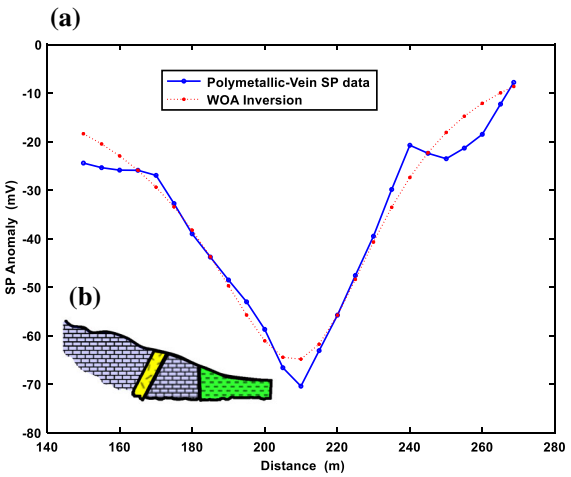


**Figure 10.** WOA inversion results for polymetallic vein SP anomaly (Eppelbaum and Khesin 2012). (**a**) Obtained response (red) and measured data (blue circles), and (**b**) inner panel sketch showing the geological setting of the polymetallic vein (redrawn from Fig. 3.28 of Eppelbaum and Khesin 2012, p. 94); (1) limestone; (2) shale; (3) polymetallic vein).

2D inclined sheet as provided by previous techniques (Jagannadha Rao et al. 1993; El-Kaliouby and Al-Garni 2009; Biswas and Sharma 2015) in Table 3.

In this study, 200 search agents and 300 iterations were conducted to carry out the WOA inversion for this example. Figure 5c demonstrates the cost function behavior with iterations. The excellent fitting between observed field and the inverted one from WOA and other methods is displayed in Figure 5b which reflected the effectiveness and stability of the WOA technique in estimation of the source unknowns. Figure 5d shows the residuals between measured SP response and the inverted anomaly from WOA and other methods in mV. Table 3 summarizes the numerical results. The obtained parameters were: $K$ = 64.62 mV, $X_a$ = – 0.455 m, $a$ = 3.35 m, $\alpha$ = 82.4° and $h$ = 7.35 m.

### *Pinggirsari Self-Potential Anomaly*

This SP anomaly was a survey associated with the presence of a fault running E–W as shown from the geological map of Garut and Pameungpeuk quadrangle, Java, Southern Bandung, Indonesia, and depicted in Figure 6a and b (modified after Alzwar et al. 1992). The SP field data (Fig. 7a) were measured in Pinggirsari village, West Java, Indonesia, on May 24, 2016. The acquired profile was laid in S–N direction to cross the fault based on the cross section from the geological map (Fig. 6c). The profile length was about 1040 m with a separation of 25 m between the measuring electrodes. In the WOA inversion process, 200 search agents and 300 iterations were used. The average best of the objective function is demonstrated in Figure 7b.

The obtained results via WOA, by Fajriani et al. (2017), and the observed data over the fault are drawn together in Figure 7a, which provided a good correlation except at the right and left sides which were not coincided with the observed data (which could be attributed to the dissimilarity in the condition of soil, either variation in fluid or porosity of the formations). Based on the measured data, it could be observed the presence of an anomaly with narrow width, which was approximated to be an attribute for the location of the shallow fault. The obtained findings contributed that the outcomes acquired by WOA were similar to those revealed by Levenberg–Marquardt method (Fajriani et al. 2017) as displayed in Table 4, where $K$ = 47.38 mV, $X_a$ = 479.625 m, $a$ = 35.85 m, $\alpha$ = – 149.98° and $h$ = 15.68 m. The residuals in (mV) between measured SP response and inverted anomaly are shown in Figure 7c.

*Surda Field Anomaly*

The geological setting of Rakha copper mines is shown in the regional geological map of the Singhbhum Shear Zone (SSZ) and location of the Mosabani and Rakha copper mines, East Singhbhum district (modified after Changkakoti et al. 1987), in Figure 8a. Figure 8b illustrates the SP profile through a line on Surda area of the Rakha mines, Singhbhum Copper Belt, in India (Murthy et al. 2005). This field example was digitized at 26 data points as input data vector for WOA inversion process, and the length of this line was about 250 m with 10-m interval. In the WOA inversion process, 200 search agents and 300 iterations were carried out. The average best of the objective function is demonstrated in Figure 8c.

The inverted parameters from WOA are displayed in Table 5 with several outcomes published by different authors (El-Kaliouby and Al-Garni 2009; Monteiro Santos 2010; Di Maio et al. 2016). The inverted SP field, computed from WOA inverted model parameters, illustrated excellent matching with the observed field data with a misfit error of 4.9%. The obtained parameters ($K$ = 94.57 mV, $X_a$ = − 4.17 m, $a$ = 29.9 m, $\alpha$ = 45.9° and $h$ = 31.3 m) contributed that the results of WOA were similar to those revealed by previous researchers. The residuals between the calculated response and the measured SP data are shown in Figure 8d.

*Bavarian Woods Field Anomaly, Germany*

A self-potential anomaly was acquired over a graphite ore body deposit which is illustrated in Figure 9a from the southern Bavarian woods, Germany (after Meiser 1962). These deposits are situated in a hercynic gneissic complex. Conformably intercalated between paragneiss and crystalline limestone of the same age, they form seams, which are to be designated as bituminous sediments of presumably Precambrian age. During the variscic orogenetic period, a folding of crystalline gneisses with predominantly E–W-striking synclines and anticlines took place and also an intrusion of granites which cross the gneisses in beds. Then again, the gneisses, limestone and granites were penetrated by a porphyritic vein sequence, so that the geological as well as the petrographical structure of the deposit is extremely complex. Generally, the graphitic veins lying between limestones and gneisess form a parallel-running sequence of lenses which are very variable in their thickness. The geological setting of this field example is depicted in Figure 9b (after Meiser 1962). The measurements were obtained at 10 m increment between the measuring locations (Meiser 1962). This field study is interpreted as 2D inclined sheet as provided by Asfahani and Tlas (2005), Sharma and Biswas (2013).

In the WOA inversion process, 100 search agents and 300 iterations are used to get the outcomes. The average best of the objective function is demonstrated in Figure 9c. The obtained parameters from WOA are as follows: $K$ = 221.0681 mV, $X_a$ = 17.026 m, $a$ = 32.523 m, $\alpha$ = 132.777° and $h$ = 49.516 m. The inverted findings suggest that the outcomes calculated by WOA are similar to those revealed by very fast simulated annealing global optimization (Sharma and Biswas 2013) as depicted in Table 6.

*Polymetallic Vein Field Anomaly, Caucasus*

This SP anomaly (Fig. 10a) is a survey acquired over a polymetallic vein, Caucasus, Northern Azerbaijan (Eppelbaum and Khesin 2012; Fig. 3.28). The polymetallic vein is conformably sandwiched through the limestone as shown in the sketch in Figure 10b (redrawn after Eppelbaum and Khesin 2012; their Fig. 3.28). The length of this profile is 120 m that was sampled at 5-m interval. This field

**Table 7.** WOA inversion results of Polymetallic Vein SP anomaly

| Methods | $K$ (mV) | $X_a$ (m) | $a$ (m) | $\alpha$ (°) | $h$ (m) |
|---|---|---|---|---|---|
| Essa and Elhussein (2017) | – | – | 0.64 | – | 30.7 |
| WOA | 113.126 | 211.437 | 4.463 | 102.124 | 30.88 |

A comparison with other method is given. The search spaces for WOA are: − 300:300 mV ($K$), 200:220 m ($X_a$), 1:10 m ($a$), 0:180° ($\alpha$) and 10:100 m ($h$)

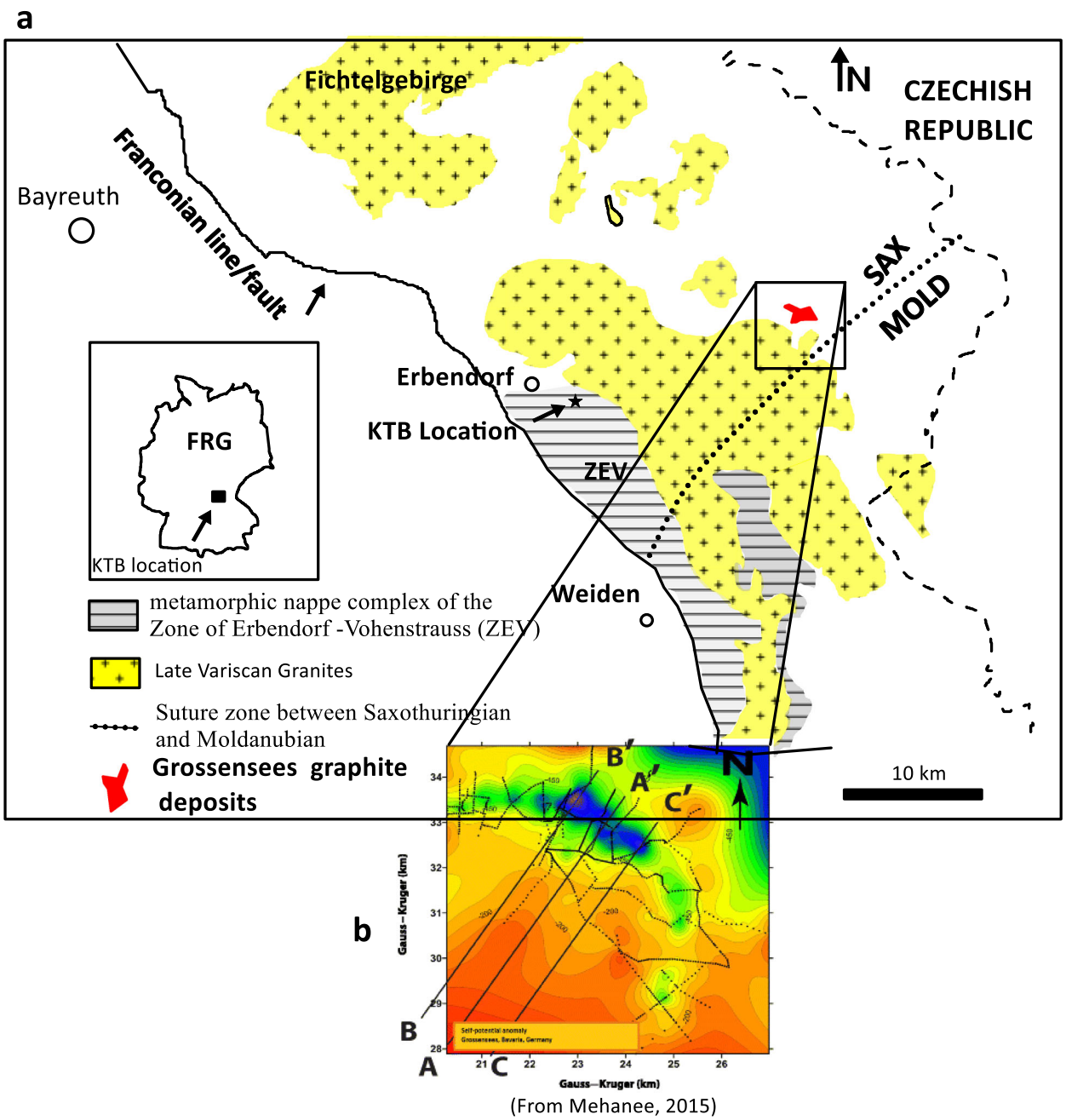


**Figure 11.** (**A**) (**a**) General geological settings around the German Continental Deep Drilling Program (KTB). The graphite deposits in Grossensees are marked in red color. (**b**) Location of the three measured profiles (from Mehanee 2015). (**B**) Left panels: WOA inversion results for Grossensees Field anomaly (Mehanee 2015). (**a**) Obtained response from WOA (red), from (Biswas 2017) (black) and measured data (blue) for profile AA″, (**b**) obtained response from WOA (red), from (Biswas 2017) (black) and measured data (blue) for profile BB″, and (**c**) obtained response from WOA (red), from (Biswas 2017) (black) and measured data (blue) for profile CC″. Right panels: Sketches showing the approximate subsurface structure for Grossensees Field anomaly. (**a**) For profile AA″, (**b**) for profile BB″, and (**c**) for profile CC″.

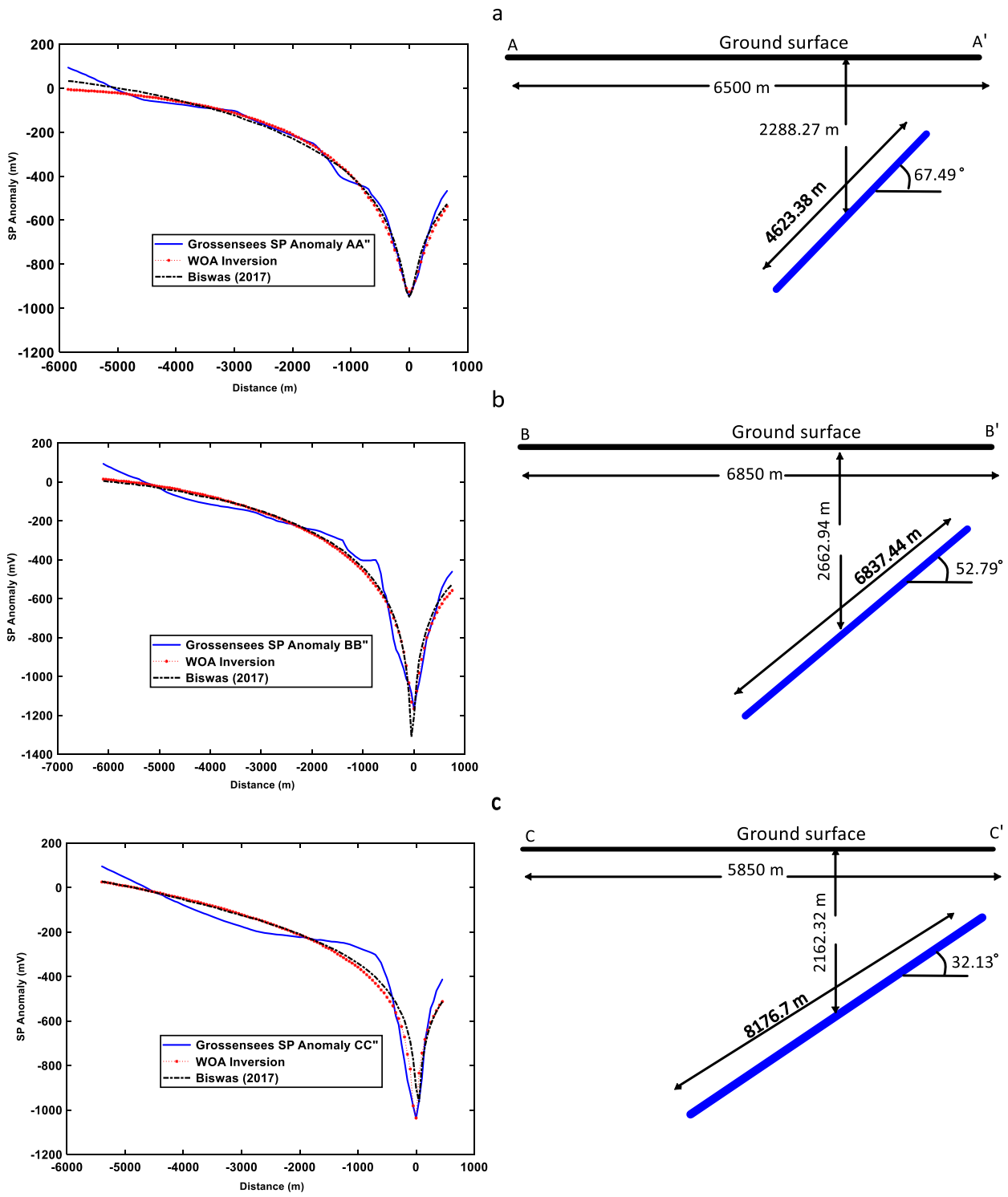


**(b)**

**Figure 11.** continued.

example has been interpreted as 2D inclined sheet by many authors (Eppelbaum and Khesin 2012, p. 94; Essa and Elhussein 2017). In the WOA inversion process, 200 search agents and 300 iterations are used to get the results. The inverted parameters obtained by WOA are $K = 113.1261$ mV, $X_a = 211.4365$ m, $a = 4.4630$ m, $\alpha = 102.124°$ and $h = 30.88$ m and in excellent correlation with those revealed by Essa and Elhussein (2017), especially the depth to the center of the sheet as depicted in Table 7.

*Grossensees Field Anomaly, Germany*

This self-potential anomaly is measured over a graphitic shear zone located in Grossensees, Germany (Stoll et al. 1995) (Fig. 11A). In the northern part of the SP anomaly map (Fig. 11A-a and b), the anomaly can be seen striking NW–SE and is related to three closures. However, it is common that for the inversion of SP data, the profile should be taken perpendicular to the strike of the anomaly [e.g., Sharma and Biswas (2013), Mehanee (2014)]. Consequently, the three profiles (AA″, BB″ and CC″) have been digitized from (Mehanee 2015) with interval equaling 20 m. There are no any available geological data, geophysical information and/or drilling data for this location contained in any published literature up to the knowledge of the present authors.

This field example has been interpreted as 2D inclined sheet by many authors (Mehanee 2015; Biswas 2017). The anomaly has been interpreted here as 2D inclined sheet type structure using WOA technique where 200 search agents and 300 iterations are used to get the results. The calculated depths to the center of the inclined sheet are found to be 2288.27, 2662.94 and 2162.32 m from profile AA″, BB″ and CC″, respectively. The calculated parameters by WOA from profile AA″ are as follows: $K = 133.117$ mV, $X_a = -867.1439$ m, $a = 2311.69$ m, $\alpha = 67.946°$ and $h = 2288.27$ m, those from profile BB″ are as follows: $K = 124.191$ mV, $X_a = -2082.072$ m, $a = 3418.72$ m, $\alpha = 52.793°$ and $h = 2662.94$ m, and those from profile CC″ are as follows: $K = 88.579$ mV, $X_a = -3483.0198$ m, $a = 4088.35$ m, $\alpha = 32.130°$ and $h = 2162.32$ m. All the three profiles with the fits between measured and inverted responses are depicted in Figure 11B (left

**Figure 12.** **A** (**b**) Detailed geological map of the border region between the German states Bavaria and Saxony and the Czech Republic with the location of the KTB borehole; BCB: Bohemian Cretaceous Basin; CB: Cheb Basin; FL: Franconian Line; HF: Hessenreuth Forest; MM: Munchberg Massif; NUPB: Northern Upper Palatinate Basin; ZEV: Zone Erbendorf-Vohenstrauß; based on the GISEurope 1:1.5 M dataset of BRGM (Modified after Cassard et al. 2008), (**a**) the measured SP anomaly (Stoll et al. 1995) overlapped on the geologic cross-section in the vicinity of the KTB-HB borehole (redrawn From Figure 6 of Stoll et al. 1995). Note that the fault system F2 extends further in depth to about 4 km (see Figure 4 in Emmermann and Lauterjung 1997). **B** WOA inversion results for KTB Field anomaly (Stoll et al. 1995). Predicted response (red) and measured data (blue) (**a**), sketch showing the approximate subsurface structure for KTB Field anomaly obtained by the trial-and-error modeling method (Stoll et al. 1995), this sketch is redrawn from Figure 5 of Stoll et al. 1995 (**b**), and as recovered by the WOA inversion technique (**c**). ▶

**Table 8.** WOA inversion results of Grossensees SP anomaly

| Methods | $K$ (mV) | $X_a$ (m) | $a$ (m) | $\alpha$ (°) | $h$ (m) |
|---|---|---|---|---|---|
| Anomaly AA″ | | | | | |
| Ranges of WOA | 10:300 | − 3000:3000 | 10:5000 | 0:90 | 10:5000 |
| Biswas (2017) | 107.5 | − 2490.2 | 3456.9 | 43.8 | 2479.6 |
| WOA | 133.117 | − 867.1439 | 2311.69 | 67.946 | 2288.27 |
| Anomaly BB″ | | | | | |
| Ranges of WOA | 10:200 | − 3000:1000 | 10:5000 | 0:180 | 10:5000 |
| Biswas (2017) | 119.8 | − 1902.2 | 3276.7 | 55.2 | 2717.6 |
| WOA | 124.191 | − 2082.072 | 3418.72 | 52.793 | 2662.94 |
| Anomaly CC″ | | | | | |
| Ranges of WOA | 10:200 | − 5000:5000 | 10:10000 | 0:90 | 10:10000 |
| Biswas (2017) | 83.1 | − 4013.9 | 4440.3 | 24.2 | 1839.1 |
| WOA | 88.579 | − 3483.0198 | 4088.35 | 32.130 | 2162.32 |

A comparison with other method is given

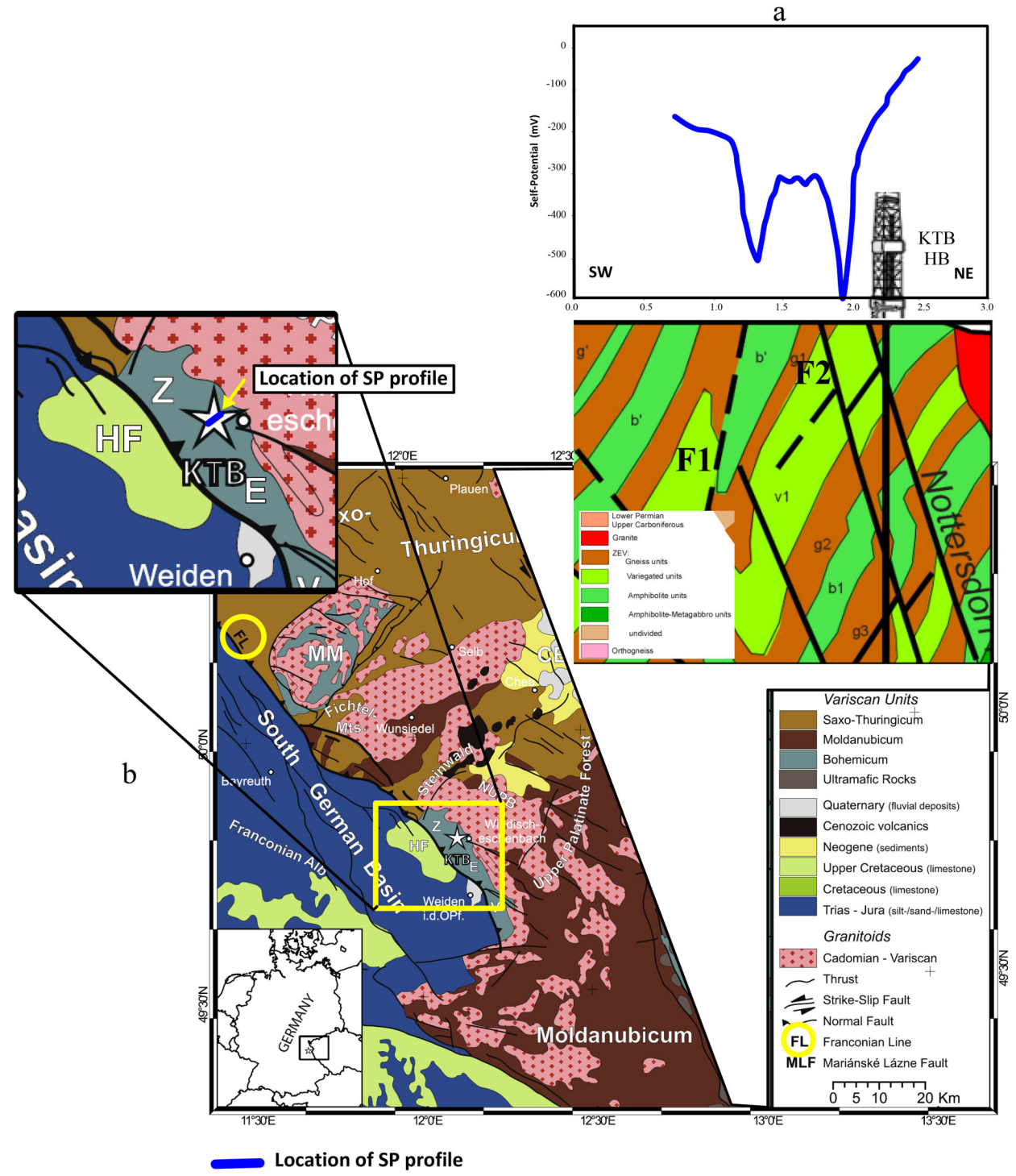
a
Self-Potential (mV)
0
-100
-200
-300
-400
-500
-600
0.0
0.5
1.0
1.5
2.0
2.5
3.0
SW
NE
KTB
HB
b
Location of SP profile
Z
HF
KTB
E
esch
Weiden
Plauen
Hof
Selb
Cheb
MM
FL
Fichtel. Mts.
Wunsiedel
Bayreuth
South German Basin
Franconian Alb
Steinwald
NTB
Windisch-eschenbach
Weiden i.d.OPf.
Upper Palatinate Forest
Moldanubicum
GERMANY
F1
F2
Nottersdorf
g'
b'
g1
v1
g2
b1
g3
Lower Permian
Upper Carboniferous
Granite
ZEV:
Gneiss units
Variegated units
Amphibolite units
Amphibolite-Metagabbro units
undivided
Orthogneiss
Variscan Units
Saxo-Thuringicum
Moldanubicum
Bohemicum
Ultramafic Rocks
Quaternary (fluvial deposits)
Cenozoic volcanics
Neogene (sediments)
Upper Cretaceous (limestone)
Cretaceous (limestone)
Trias - Jura (silt-/sand-/limestone)
Granitoids
Cadomian - Variscan
Thrust
Strike-Slip Fault
Normal Fault
FL Franconian Line
MLF Mariánské Lázne Fault
0 5 10 20 Km
50°0N
49°30N
11°30E
12°0E
12°30E
13°0E
13°30E
Location of SP profile

(A)

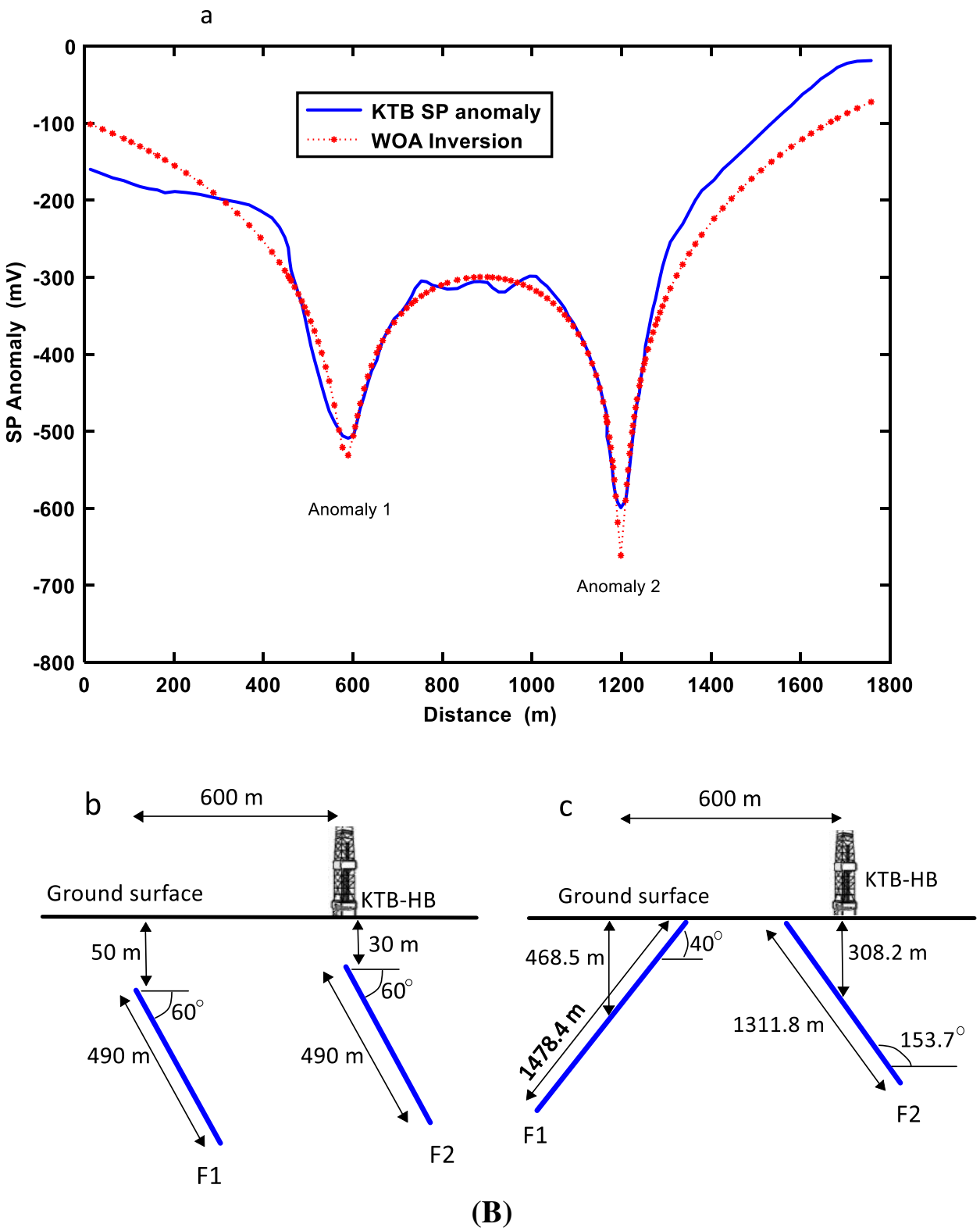


(B)

**Figure 12.** continued.

**Table 9.** WOA inversion results of KTB SP anomaly

| Method | $K$ (mV) | $X_a$ (m) | $a$ (m) | $\alpha$ (°) | $h$ (m) |
|---|---|---|---|---|---|
| Source #1 | | | | | |
| Ranges of WOA | 10:200 | 500:700 | 10:2000 | 40:80 | 10:500 |
| WOA | 58.6277 | 632.704 | 739.248 | 40.0219 | 468.535 |
| Source #2 | | | | | |
| Ranges of WOA | 10:200 | 1100:1300 | 10:2000 | 60:180 | 10:500 |
| WOA | 54.530 | 1173.5613 | 655.924 | 153.758 | 308.208 |

panels). The subsurface structure obtained by WOA is shown in Figure 11B-a, b, and c (right panels). Table 8 shows the calculated model parameters using WOA together with those of Biswas (2017).

*KTB Borehole Field Anomaly, Germany*

Through the zone of Erbendorf-Vohenstrauß (ZEV) in the northern part of Oberpfalz (NE Bavaria, Germany), two boreholes were drilled for research during the German Continental Deep Drilling Program that went to the Variscan basement (Franke 1989; Gobashy et al. 1993a, b, c; Bosum et al. 1993; Bigalke and Grabner 1997; Kontny et al. 1997). The first borehole, the KTB-VB, went to a depth of about 4 km, and the second one KTB-HB, which was drilled to nearly 9.1 km deep, was around 200 m distance separated between the two boreholes (Emmermann and Lauterjung 1997).

The graphite occurrence is related to a number of steeply inclined shear plates according to the data of the two boreholes, and the thickness of the graphitic layers is of a few millimeters (Stoll et al. 1995; ELEKTB Group 1997). The Franconian fault system (shown in the geological map in Fig. 12A (after Cassard et al. 2008) distinguished the rocks of the ZEV from the Permo-Mesozoic sedimentary basin, has a strike (NW–SE) and a dip direction to NE, and intersects at a depth of around 7 km with the KTB borehole (Kontny et al. 1997).

This SP anomaly (Fig. 12A-a and b) was measured near the KTB boreholes (Stoll et al. 1995). This profile has two negative peak zones (anomaly 1 of magnitude equals − 500 mV and anomaly 2 of magnitude equals − 600 mV) and was analyzed by many authors (Stoll et al. 1995; Srivastava and Agarwal 2009; Dmitriev 2012; Mehanee 2015). This anomaly has been interpreted here as multiple 2D inclined sheets [i.e., two inclined sheets instead of dividing it to a two separate anomalies and apply inversion for each one alone as made by Mehanee (2015), Biswas (2017)] using WOA technique where 500 search agents and 700 iterations are used to obtain the results. The predicted and measured response is depicted in Figure 12B-a. The misfit error between the calculated and the observed anomaly is about 4.6%, which is less than that provided by Mehanee (2015) as 9.26 and 6.82% for anomaly 1 and anomaly 2, respectively. This profile was interpreted by Stoll et al. (1995) via 2D trial-and-error modeling that fitted the two negative peaks to two inclined electric conductors like sheets. The obtained subsurface structure by Stoll et al. (1995) is depicted in Figure 12B-b; F1 and F2 represent interpreted sheet models for anomaly 1 and anomaly 2, respectively, and that obtained by WOA is displayed in Figure 12B-c and was in excellent correlation with those of the inclined shear planes obtained from geophysical research and confirmed with drilling where graphitization has occurred as shown in Figure 12A-a. The inverted parameters obtained by WOA are $K = 58.6277$ mV, $X_a = 632.704$ m, $a = 739.248$ m, $\alpha = 40.0219°$ and $h = 468.535$ m for anomaly 1 and are $K = 54.530$ mV, $X_a = 1173.5613$ m, $a = 655.924$ m, $\alpha = 153.758°$ and $h = 308.208$ m for anomaly 2. These analyses show that WOA technique can provide reliable inversion outcomes when applied to measured SP data resulted from multi-sources via solving multi-objective function to get the inverted parameters. Table 9 shows the inverted model parameters using WOA.

## CONCLUSION

In this work, investigation was carried out for WOA as a meta-heuristic algorithm to solve the inverse problem of self-potential resulted from 2D inclined sheet which is a common model in mineral exploration and shear zones. WOA inversion was applied to solve for five SP unknowns which are the polarization amplitude ($K$), the zero distance from

origin ($x_a$), the depth to the sheet center ($h$), the polarization angle ($\alpha$) and the half-width of the sheet ($a$). It was tested on noise-free synthetic example and on noisy example, where it showed good results and stability until 30% noise. Moreover, when comparing with other global optimizers, a clear consistency can be observed between the WOA's calculated parameters and the true ones, leading to the lowest misfit error (0.03%) in the studied model. This confirms that WOA has significant improvements in its stability and consistency.

The outcomes from WOA inversion of the several real examples over different mineralized zones and paleo-shears showed good fits with those published in the literature. The real studies collectively along with the synthetic examples have reflected the competence of the WOA. The results showed the stability of WOA as a global optimizer compared with the traditional local search techniques. It is noteworthy that it provided sufficient and accurate results even though the search range was wide compared with the local methods that need the initial solution to be very close to the real one; otherwise, their solution may be trapped in the local minimum region. Therefore, this research suggested WOA as an excellent and easily applicable technique, especially for mineral exploration, tracing paleo-shear zones and generally over SP anomalous zones.

## REFERENCES


Abdelazeem, M., & Gobashy, M. (2006). Self-potential inversion using genetic algorithm. *JKAU Earth Science, 17,* 83–101.

Abdelrahman, E. M., Ammar, A. A., Hassanein, H. I., & Hafez, M. A. (1998). Derivative analysis of SP anomalies. *Geophysics, 63*(3), 890–897. https://doi.org/10.1190/1.1444399.

Abdelrahman, E. M., El-Araby, H. M., Hassaneen, A. G., & Hafez, M. A. (2003). New methods for shape and depth determinations from SP data. *Geophysics, 68*(4), 1202–1210. https://doi.org/10.1190/1.1598112.

Alzwar, M., Akbar, N., & Bachri, S. (1992). Peta Geologi Lembar Garut dan Pameungpeuk. Jawa Pusat Penelitian dan Pengembangan Geologi.

Arora, T., Linde, N., Revil, A., & Castermant, J. (2007). Non-intrusive characterization of the redox potential of landfill leachate plumes from self-potential data. *Journal of Contaminant Hydrology, 92,* 274–292.

Asfahani, J., & Tlas, M. (2005). A constrained nonlinear inversion approach to quantitative interpretation of self-potential anomalies caused by cylinders, spheres and sheet-like structures. *Pure and Applied Geophysics, 162,* 609–624. https://doi.org/10.1007/s00024-004-2624-0.

Atchuta Rao, D., & Ram Babu, H. V. (1983). Quantitative interpretation of self-potentialanomalies due to two-dimensional sheet-like bodies. *Geophysics, 48*(12), 1659–1664.

Babu, H. V. R., & Rao, D. A. (1988). A rapid graphical method for the interpretation of the self potential anomaly over a two-dimensional inclined sheet of finite depth extent. *Geophysics, 53,* 1126–1128.

Bigalke, J., & Grabner, E. W. (1997). The geobattery model: A contribution to large scale electrochemistry. *Electrochimica Acta, 42*(23–24), 3443–3452.

Biswas, A. (2017). A review on modeling, inversion and interpretation of self-potential in mineral exploration and tracing paleo-shear zones. *Ore Geology Reviews, 91,* 21–56.

Biswas, A. (2019). Inversion of amplitude from the 2D analytic signal of self-potential anomalies. In K. Essa (Ed.), *Minerals*. London: In Tech Education and Publishing. ISBN 978-953-51-6784-6.

Biswas, A., & Sharma, S. P. (2016). Interpretation of Self-potential anomaly over 2-D inclined thick sheet structures and analysis of uncertainty using very fast simulated annealing global optimization. *Acta Geodaetica et Geophysica, 52*(4), 439–455.

Biswas, A., & Sharma, S. P. (2015). Interpretation of self-potential anomaly over idealized body and analysis of ambiguity using very fast simulated annealing global optimization. *Near Surface Geophysics, 13*(2), 179–195.

Biswas, A., & Sharma, S. P. (2014a). Optimization of self-potential interpretation of 2-D inclined sheet-type structures based on very fast simulated annealing and analysis of ambiguity. *Journal of Applied Geophysics, 105,* 235–247.

Biswas, A., & Sharma, S. P. (2014b). Resolution of multiple sheet-type structures in self-potential measurement. *Journal of Earth System Science, 123*(4), 809–825.

Black, W. E., & Corwin, R. F. (1984). Application of self-potential measurements to the delineation of groundwater seepage in earth-fill embankments. *Society of Exploration Geophysicists Technical Program Expanded Abstracts, 3,* 162–164.

Bosum, W., Casten, U., Fieberg, F., Goetze, H.-J., Gobashy, M., et al. (1993). *Gravity and magnetic structural models of the KTB-area. Part B: geoscientific investigations*. KTB report 93-2, 319-322, Hannover.

Cassard, D., Billa, M., & Deschamps, Y. (2008). *Map of the main mineral deposits of Europe—an extract from GIS Europe*. Report BRGM/RP-56464-FR.

Changkakoti, A., Gray, J., Morton, R. D., & Sarkar, S. N. (1987). The Mosabani Copper Deposit, India—A preliminary study of nature and genesis of the ore fluids. *Economic Geology, 82,* 1619–1625.

Di Maio, R., Rani, P., Piegari, E., & Milano, L. (2016). Self-potential data inversion through a genetic-price algorithm. *Computers & Geosciences, 94,* 86–95. https://doi.org/10.1016/j.cageo.2016.06.005.

Dmitriev, A. N. (2012). Forward and inverse self-potential modeling: A new approach. *Russian Geology and Geophysics, 53,* 611–622.

Drahor, M. G. (2004). Application of the self-potential method to archaeological prospection: Some case histories. *Archaeological Prospection, 11,* 77–105.

Drahor, M. G., Akyol, A. L., & Dilaver, N. (1996). An application of the self-potential (SP) method in archaeogeophysical prospection. *Archaeol. Prospect., 3,* 141–158.

El-Araby, H. M. (2004). A new method for complete quantitative interpretation of self-potential anomalies. *Journal of Applied Geophysics, 55,* 211–224.

ELEKTB Group. (1997). KTB and the electrical conductivity of the crust. *Journal of Geophysical Research: Solid Earth, 102*(B8), 18289–18305.

El-Kaliouby, H. M., & Al-Garni, M. A. (2009). Inversion of self-potential anomalies caused by 2D inclined sheets using

neural networks. *Journal of Geophysics and Engineering, 6,* 29–34. https://doi.org/10.1088/17422132/6/1/003.

Emmermann, R., & Lauterjung, J. (1997). The German continental deep drilling program KTB: Overview and major results. *Journal of Geophysical Research: Solid Earth, 102*(B8), 18179–18201.

Eppelbaum, L., & Khesin, B. (2012). Methodological specificities of geophysical studies in the complex environments of the Caucasus. In L. Eppelbaum & B. Khesin (Eds.), *Geophysical studies in the caucasus* (pp. 39–138). Berlin: Springer.

Essa, K. S., & Elhussein, M. (2017). A new approach for the interpretation of self-potential data by 2-D inclined plate. *Journal of Applied Geophysics, 136,* 455–461.

Fajriani, V., Srigutomo, W., & Pratomo, P. M. (2017). Interpretation of self-potential anomalies for investigating fault using the Levenberg–Marquardt method: A study case in Pinggirsari, West Java, Indonesia. *IOP Conference Series: Earth and Environmental Science*. https://doi.org/10.1088/1755-1315/62/1/012004.

Franke, W. (1989). The geological framework of the KTB drill site, Oberpfalz. In R. Emmermann & J. Wohlenberg (Eds.), *The German continental drilling program (KTB)* (pp. 37–54). New York: Springer.

Gobashy, M. M., Casten, U., & Neubauer, F. M. (1993a). Ergebnisse der Borlochgravimetrie in der KTB-Hauptbohrung und einneues Strukturmodell: Proceeding of the DeutchenGeophysikalichen Gesellschaft (DGG), 22–27 March, Kiel, West Germany.

Gobashy, M. M., Casten, U., & Neubauer, F. M. (1993b). A final report on the interpretation of the BHGM gravity measurements in the KTB-main well, Windischeschenbach, Germany. A final report presented to the DFG, August 1993.

Gobashy, M. M., Casten, U., & Neubauer, F. M. (1993c). *Borehole gravimetry in the KTB-main well and a new structural interpretation. Part B: Geoscientific investigations*. KTB report 93-2, 357-360, Hannover.

Göktürkler, G., & Balkaya, Ç. (2012). Inversion of self-potential anomalies caused by simple geometry bodies using global optimization algorithms. *Journal of Geophysics and Engineering, 9,* 498–507.

Guptasarma, D. (1983). Effect of surface polarization on resistivity modeling. *Geophysics, 48*(1), 98–106. https://doi.org/10.1190/1.1441411.

Jagannadha Rao, S., Rama Rao, P., & Radhakrishna Murthy, I. V. (1993). Automatic inversion of self-potential anomalies of sheet-like bodies. *Computers & Geosciences, 19,* 61–73.

Kher, S. V., & Peshwa, V. V. (1989). The geology and structure of the area south of Gani, Kurnool district, Andhra Pradesh—A study based on remotely sensed data. *Journal of the Indian Society of Remote Sensing, 17*(4), 61–67.

Kontny, A., Friedrich, G., Behr, H. J., de Wall, H., Horn, E. E., Moller, P., et al. (1997). Formation of ore minerals in metamorphic rocks of the German continental deep drilling site (KTB). *Journal of Geophysical Research: Solid Earth, 102*(8), 18323–18336.

Li, X., & Yin, M. (2012). Application of differential evolution algorithm on self-potential data. *PLoS ONE*. https://doi.org/10.1371/journal.pone.0051199.

Mehanee, S. (2014). An efficient regularized inversion approach for self-potential data interpretation of ore exploration using a mix of logarithmic and non-logarithmic model parameters. *Ore Geology Reviews, 57,* 87–115.

Mehanee, S. (2015). Tracing of paleo-shear zones by self-potential data inversion: Case studies from the KTB, Rittsteig, and Grossensees graphite-bearing fault planes. *Earth Planets Space, 67,* 14–47.

Meiser, P. (1962). A method of quantitative interpretation of self-potential measurements. *Geophysical Prospecting, 10,* 203–218.

Mendonca, C. A. (2008). Forward and inverse self-potential modeling in mineral exploration. *Geophysics, 73,* F33–F43.

Mirjalili, S., & Lewis, A. (2016). The Whale optimization algorithm. *Advances in Engineering Software, 95,* 51–67. https://doi.org/10.1016/j.advengsoft.2016.01.008.

Monteiro Santos, F. A. (2010). Inversion of self-potential of idealized bodies' anomalies using particle swarm optimization. *Computers & Geosciences, 36,* 1185–1190.

Moore, J. R., Boleve, A., Sanders, J. W., & Glaser, S. D. (2011). Self-potential investigation of moraine dam seepage. *Journal of Applied Geophysics, 74,* 277–286.

Murty, B. V. S., & Haricharan, P. (1984). SP anomaly over doable line of poles-interpretation through log curves. *Journal of Earth System Science, 93,* 437–445.

Murty, B. V. S., & Haricharan, P. (1985). Nomogram for the spontaneous potential profile over sheet-like and cylindrical two-dimensional sources. *Geophysics, 50,* 1127–1135.

Murthy, I. V. R., Sudhakar, K. S., & Rao, P. R. (2005). A new method of interpreting self potential anomalies of two-dimensional inclined sheets. *Computers & Geosciences, 31,* 661–665.

Paul, M. K. (1965). Direct interpretation of self-potential anomalies caused by inclined sheets of infinite horizontal extensions. *Geophysics, 30,* 418–423.

Ramam, P. K., & Murty, V. N. (1997). *Geology of Andhra Pradesh*. Bangalore: Geological Society of India.

Rani, P., Di Maio, R., & Piegari, E. (2015). High-resolution spectral analysis methods for self-potential data inversion. In *Expanded abstract volume of the 85th SEG annual meeting and exposition* (pp. 1596–1601). New Orleans.

Rao, R. M., Babu, H., & Sivakumar Sinha, G. (1982). A Fourier transform for the interpretation of self-potential anomalies due to two-dimensional inclined sheet of finite depth. *Pure and Applied Geophysics, 120,* 365–374.

Sanker Narayan, P. V., Sarma, S. V. S., Rao, D. A., Jain, S. C., Verma, S. K., et al. (1982). Report on multiparameter geophysical experiment in Kalava area (Cuddapah Basin) Kurnool District, Andhra Pradesh. *Paper presented at the fifth workshop on status, problems and programmes in Cuddapah Basin, held during 11–12th January, 1982*, organized by the Institute of Indian Peninsular Geology, Hyderabad, India.

Sharma, S. P., & Biswas, A. (2013). Interpretation of self-potential anomaly over 2D inclined structure using very fast simulated annealing global optimization—an insight about ambiguity. *Geophysics, 78*(3), 3–15.

Shi, W., & Morgan, F. D. (1996). Non-uniqueness in self-potential inversion. *Society of Exploration Geophysicists Expanded Abstracts, 15,* 950–953. https://doi.org/10.1190/1.1826817.

Srivastava, S., & Agarwal, B. N. P. (2009). Interpretation of self-potential anomalies by enhanced local wave number technique. *Journal of Applied Geophysics, 68,* 259–268.

Stoll, J., Bigalke, J., & Grabner, E. W. (1995). Electrochemical modelling of self-potential anomalies. *Surveys In Geophysics, 16,* 107–120.

Sundararajan, N., Srinivasa Rao, P., & Sunitha, V. (1998). An analytical method to interpret self-potential anomalies caused by 2D inclined sheets. *Geophysics, 63,* 1551–1555.

Sungkono, D. D. (2018). Black hole algorithm for determining model parameter in self-potential data. *Journal of Applied Geophysics, 148,* 189–200.

Titov, K., Konosavsky, P., & Narbut, M. (2015). Pumping test in a layered aquifer: Numerical analysis of self-potential signals. *Journal of Applied Geophysics, 123,* 188–193. https://doi.org/10.1016/j.jappgeo.2015.10.006.

Zlotnicki, J., & Nishida, Y. (2003). Review on morphological insights of self-potential anomalies on volcanoes. *Surveys In Geophysics, 24,* 291–338.